MoCoSR: Respiratory Motion Correction and Super-Resolution for 3D Abdominal MRI

Weitong Zhang[1,2(✉)], Berke Basaran[1,2,3], Qingjie Meng[2], Matthew Baugh[2], Jonathan Stelter[7], Phillip Lung[6], Uday Patel[6], Wenjia Bai[2,3,4], Dimitrios Karampinos[7], and Bernhard Kainz[2,5]

[1] UKRI CDT in AI for Healthcare, Imperial College London, London, UK
weitong.zhang20@imperial.ac.uk
[2] Department of Computing, Imperial College London, London, UK
[3] Data Science Institute, Imperial College London, London, UK
[4] Department of Brain Sciences, Imperial College London, London, UK
[5] Friedrich-Alexander University Erlangen-Nürnberg, Erlangen, DE, Germany
[6] St Mark' Radiology, London North West University Healthcare NHS Trust, London, UK
[7] Department of Diagnostic and Interventional Radiology, Technical University of Munich, Munich, Germany

Abstract. Abdominal MRI is critical for diagnosing a wide variety of diseases. However, due to respiratory motion and other organ motions, it is challenging to obtain motion-free and isotropic MRI for clinical diagnosis. Imaging patients with inflammatory bowel disease (IBD) can be especially problematic, owing to involuntary bowel movements and difficulties with long breath-holds during acquisition. Therefore, this paper proposes a deep adversarial super-resolution (SR) reconstruction approach to address the problem of multi-task degradation by utilizing cycle consistency in a staged reconstruction model. We leverage a low-resolution (LR) latent space for motion correction, followed by super-resolution reconstruction, compensating for imaging artefacts caused by respiratory motion and spontaneous bowel movements. This alleviates the need for semantic knowledge about the intestines and paired data. Both are examined through variations of our proposed approach and we compare them to conventional, model-based, and learning-based MC and SR methods. Learned image reconstruction approaches are believed to occasionally hide disease signs. We investigate this hypothesis by evaluating a downstream task, automatically scoring IBD in the area of the terminal ileum on the reconstructed images and show evidence that our method does not suffer a synthetic domain bias.

Keywords: Abdominal MR · Motion Correction · Super-resolution · Deep Learning

Supplementary Information The online version contains supplementary material available at https://doi.org/10.1007/978-3-031-43999-5_12.

H. Greenspan et al. (Eds.): MICCAI 2023, LNCS 14229, pp. 121–131, 2023.
https://doi.org/10.1007/978-3-031-43999-5_12

1 Introduction

Inflammatory bowel disease (IBD) is a relatively common, but easily overlooked disease. Its insidious clinical presentation [1] can lead to a long delay between the initial causative event and the diagnosis [2]. One of its manifestations, Crohn's disease, often exhibits symptoms such as abdominal pain, diarrhoea, fatigue, and cramping pain, which can be accompanied by severe complications [3]. Although Crohn's disease cannot be completely cured, early diagnosis can significantly reduce treatment costs and permanent physical damage [4]. MRI plays a crucial role in diagnosing and monitoring Crohn's disease. In clinical applications and research, high-resolution (HR) MRI is often preferred over endoscopy as it is non-invasive and visualises more details for the small bowel. MRI is preferred over computed tomography (CT) imaging as it does not use radiation, which is an important consideration in younger patients. Unfortunately, MR acquisition for patients with Crohn's disease can easily become compromised by respiratory motion.

As a result, many patients' images are degraded by respiration, involuntary movements and peristalsis. Furthermore, due to technical limitations, it is difficult to acquire HR images in all scan orientations. This limits the assessment of the complete volume in 3D. Given these problems, we aim to develop a novel method that can perform both motion correction (MC) and super-resolution (SR) to improve the quality of 3D IBD MRI and to support accurate interpretation and diagnosis.

Motion can cause multiple issues for MR acquisition. Abdominal MRI scans are usually 2D multi-slice acquisitions [5]. As a result, 3D bowel motion can lead to intra- and inter-plane corruptions [6], *e.g.*, slice misregistration, slice profile effects, and anisotropic spatial resolution. SR can be used to enhance these scans, but conventional methods often struggle with this type of anisotropic data or may unintentionally hide significant imaging findings.

Despite these challenges, MC and SR are crucial because corrupted MR images can lead to inaccurate interpretation and diagnosis [7]. Manual correction or enhancement of these volumes is not feasible.

Contribution: Our method (MoCoSR) alleviates the need for semantic knowledge and manual paired-annotation of individual structures and the requirement for acquiring multiple image stacks from different orientations, *e.g.*, [8].

There are several methodological contributions of our work: (1) First, to account for non-isotropic voxel sizes of abdominal images, we reconstruct spatial resolution from corrupted bowel MR images by enforcing cycle consistency. (2) Second, volumes are corrected by incorporating latent features in the LR domain. The complementary spatial information from unpaired quality images is exploited via cycle regularisation to provide an explicit constraint. Third, we conduct extensive evaluations on 200 subjects from a UK Crohn's disease study, and a public abdominal MRI dataset with realistic respiratory motion. (3) Experimental evaluation and analysis show that our MoCoSR is able to generate high-quality MR images and performs favourably against other, alter-

native methods. Furthermore, we explore confidence in the generated data and improvements to the diagnostic process. (4) Experiments with existing models for predicting the degree of small bowel inflammation in Crohn's disease patients show that MoCoSR can retain diagnostically relevant features and maintain the original HR feature distribution for downstream image analysis tasks.

Related Work: MRI SR. For learning-based MRI super-resolution, [9] discussed the feasibility of learning-based SR methods, where encoder-decoder methods [10–12] are commonly used to model a variety of complex structures while preserving details. Most single-forward [13–15] and adversarial methods [16,17] rely on paired data to learn the mapping and degradation processes, which is not acceptable in real-world scenarios where data are mismatched. [18] utilizes cyclic consistency structures to address unpaired degradation adaptation in brain SR, however abdominal data would be more complicated and suffer from motion corruption. Joint optimization of MC and SR remains challenging because of the high-dimensionality of HR image space, and LR latent space has been introduced in order to alleviate this issue. Recent studies on SR joint with other tasks (*e.g.*, reconstruction, denoising) have demonstrated improvements in the LR space [11,19,20]. For this purpose, we utilize a cycle consistency framework to handle unpaired data and joint tasks.

Automated Evaluation of IBD. In the field of machine learning and gastrointestinal disease, [21] used random forests to segment diseased intestines, which is the first time that image analysis support has been applied to bowel MRI. However, this technique requires radiologists to label and evaluate diseased bowel segments, and patients' scan times are long. In [22] residual networks focused on the terminal ileum to detect Crohn's disease. In this case, quality reconstruction data is extremely important for the detection of relevant structures.

2 Method

Problem Formulation and Preliminaries: In 3D SR, the degradation process is modeled with: $I_{LR} = \mathcal{D}(I_{HR}; k_I, \downarrow_s) + n$, $\mathcal{D}()$ represents the downsampling with the blur kernel k_I, scaling factor s, and noise n. In this work, we propose the motion corruption term M, which operates on LR latent space. And our MC-SR model can be refined to

$$I_{LR} = M(\mathcal{D}(I_{HR}; k_I, \downarrow_s); Z) + n \tag{1}$$

MoCoSR Concept: As shown in Fig. 1, our multi-task framework consists of three parts: a pair of corrupted LR (CLR) encoder and SR decoder on corrupted LR input, a pair of quality SR (QLR) encoder and learned LR (LLR) decoder on HR input and two task-specific discriminators. For the first two pairs, individual features are extracted and scaling is applied to provide our network with the ability to handle multiple tasks at different scales. The discriminators are then used to identify features for each scale.

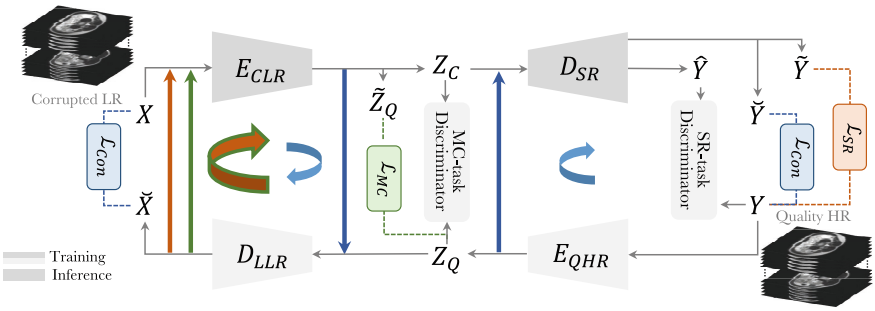

Fig. 1. During training, the input comprises corrupted MRI with motion artifacts and blurring effects. During inference, only the first pair of LR encoder E_{CLR} and SR decoder D_{SR} will be utilized to generate high-quality, motion-free, and super-resolved images.

A quality HR volume Y is fed first into the QHR encoder in order to obtain a quality latent feature map Z_Q upon which the corrupted LR can be trained. due to the unpaired scenario. For MC, Z_Q passes to LLR and CLR to gain $\tilde{Z}_Q$ with $\mathcal{L}_{MC}$, where LLR learns the corruption feature and degradation, and CLR encodes the multi-degradation from the corrupted LR input X. For SR, $\tilde{Y}$ is then generated after the SR decoder and ensure the SR purpose with $\mathcal{L}_{SR}$. To ensure training stability, two consistency loss functions $\mathcal{L}_{Con}$ are utilized for each resolution space. The arrows indicate the flow of the tasks. A pair of task-specific discriminators is used to improve the performance of each task-related encoder and decoder.

Loss Functions: Rather than aiming to reconstruct motion-free and HR images in high dimensional space with paired data, we propose to regularize in low dimensional latent space to obtain a high quality LR feature that can be used for upscaling. A $\mathcal{L}_{MC}$ between $\tilde{Z}_Q$ downsampled from QHR and Z_Q cycled after LLR and CLR, defines in an unpaired manner as follows:

$$\mathcal{L}_{MC} = E\left[\left|Z_Q - \tilde{Z}_Q\right|\right] \tag{2}$$

As the ultimate goal, SR focuses on the recovery and upscaling of detailed high-frequency feature, $\mathcal{L}_{SR}$ is proposed to optimize the reconstruction capability by passing through cycles at various spaces:

$$\mathcal{L}_{SR} = \mathcal{L}_1(Y, \tilde{Y}) \tag{3}$$

The dual adversarial $\mathcal{L}_{DAdv}$ is applied to improve the generation capability of the two sets of single generating processes in the cyclic network:

$$\mathcal{L}_{DAdv} = \mathcal{L}_{adv}(\breve{X}) + \mathcal{L}_{adv}(\breve{Y}) + \mathcal{L}_{adv}(\tilde{Y}) \tag{4}$$

The corresponding two task-specific discriminators $\mathcal{L}_{DMC}$ and $\mathcal{L}_{DSR}$ for discriminating between corrupted and quality images followed are used for the

purpose of staged reconstruction Z_Q and $\hat{Y}$ of MC at latent space and SR at spatial space, respectively. Furthermore, a joint cycle consistency loss is used to improve the stability of training in both spaces:

$$\mathcal{L}_{Con} = \mathcal{L}_1(X, \check{X}) + \mathcal{L}_1(Y, \check{Y}) \tag{5}$$

For MoCoSR generators, the joint loss function is finally defined as follows:

$$\mathcal{L} = \mathcal{L}_{SR} + \lambda_1 \mathcal{L}_{MC} + \lambda_2 \mathcal{L}_{DAdv} + \lambda_3 \mathcal{L}_{Con} \tag{6}$$

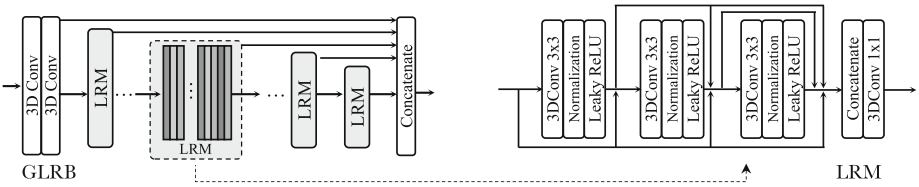

Fig. 2. GLRB is used to construct an effective feature extraction backbone based on encoders and decoders with different inputs. Additionally, the SR decoder and the QHR encoder include additional Pixel-shuffle and downsampling layers.

Network Architecture: In the paired encoder-decoder structure, we developed a 3D Global and Local Residual Blocks (GLRB) with Local Residual Modules (LRM) in Fig. 2 based on [23]. The GLRB is designed to extract local features and global structural information at 3D level, and then construct blocks for multi-scale features connected to the output of the first layer. The residual output is then added to the input using a residual connection to obtain a staged output. The model implements the extraction of local features while integrating all previous features through the connected blocks and compression layers. The decoders are employed with the upsampling prior to the convolution layers.

3 Experiments

Data Degradation: We use $64 \times 64 \times 64$ patches. For downsampling and the degradation associated with MRI scanning, (1) Gaussian noise with a standard deviation of 0.25 was added to the image. (2) Truncation at the k-space, retaining only the central region of the data. On top of this, we have developed a motion simulation process to represent the pseudo-periodic multi-factor respiratory motion (PMRM) that occurs during scanning, as shown in Fig. 3 (a). The simulated motion includes the influence of environmental factors that cause the respiratory intensity and frequency to fluctuate within a certain range. This lead to the presence of inter-slice misalignment in image domains.

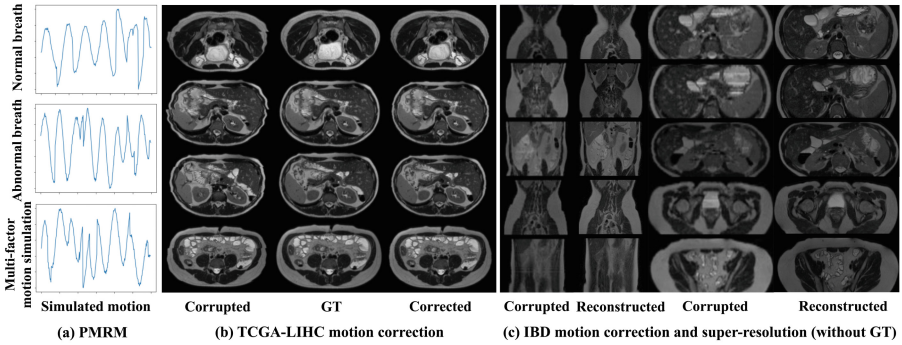

Fig. 3. (a) The proposed PMRM sequence of respiratory simulation for motion corruption for Crohn's diseases. (b) The staged reconstruction process involving application of PMRM, MC result, and ground truth (GT) on TCGA-LIHC dataset. The MC matrix is calculated and applied on HR for visual comparison with simulated motion perturbations directly. (c) The MoCoSR results on clinical IBD data without GT.

TCGA-LIHC Data Set, Abdominal MRI: A total of 237 MR exams are collected from The Cancer Imaging Archive Liver Hepatocellular Carcinoma (TCGA-LIHC). The data contains 908 MRI series from 97 patients. We applied simulated motion to TCGA MRI-Abdomen series to generate the motion-corrupted dataset with respiration-induced shift.

IBD Data Set, Inflammatory Bowel Disease: MRI sequences obtained include axial T2 images, coronal T2 images and axial postcontrast MRI data on a Philips Achieva 1.5 T MR scanner. Abdominal 2D-acquired images exhibit motion shifts between slices and fibrillation artefacts due to the difficulty of holding one's breath/body movement and suppressing random organ motion for extended periods. The dataset contains 200 available sample cases with four classes, healthy, mild, moderate, and severe small bowel Crohn's disease inflammation as shown in Table 1. The abnormal Crohn's disease sample cases, which could contain more than one segment of terminal ileum and small bowel Crohn's disease, were defined based on the review of clinical endoscopic, histological, and radiological images and by unanimous review by the same two radiologists (this criterion has been used in the recent METRIC trial investigating imaging in Crohn's disease [24]).

Setting: We compare with interpolation of bicubic and bilinear techniques, rapid and accurate MR image SR (RAISR-MR) with hashing-based learning [25], which we use as the representative of the model-based methods, and MRI SR with various generative adversarial networks (MRESR [17], CMRSR [16]) as the learning-based representatives. For training, with train/val/test with 70%/10%/20%. Various methods were included in the quantitative evaluation, including single forward WGAN (S-WGAN) and cycle RDB (C-RDB) for ablation experiments on the cycle consistency framework and the GLRB setting.

Table 1. IBD data set: the upper shows MRI data acquisition parameters. The lower shows the number of patients in each severity level of inflammation.

Planes	Sequence	TR [ms]/TE [ms]	Matrix	Slice [mm]	FOV	Time [s]
Axial	T1 FFE (e-THRIVE)	5.9/3.4	$512 \times 512 \times 96$	3.00	375	20.7×2
Axial Postcon	single-shot T2 TSE	587/120	$528 \times 528 \times 72$	3.50	375	22.3×2
Coronal	single-shot T2 TSE	554/120	$512 \times 512 \times 34$	3.00	375	21.1
Inflammation class		Healthy	Mild	Moderate	Severe	
Number of patients		100	49	42	9	

Table 2. Quantitative evaluation of extensive methods on TCGA-LIHC and IBD data sets in terms of SSIM and PSNR for 3D abdominal MRI SR

Method	TCGA-LIHC upper abdominal		IBD lower abdominal	
	SSIM ↑	PSNR ↑	SSIM ↑	PSNR ↑
Bicubic	0.8166	28.53	0.6582	25.30
Bilinear	0.8219	29.15	0.6749	26.27
RAISR-MR [25]	0.8940	32.24	0.8512	31.53
MRESR [17]	0.9042	33.74	0.8529	30.60
CMRSR [16]	0.9185	35.92	0.8662	32.90
S-WGAN	0.8521	30.91	0.7313	28.19
C-RDB	0.9102	35.15	0.8624	32.78
MoCoSR (C-GLRB)	0.9257	35.67	0.8719	33.56

Results: The quantitative results are presented in Table 2 on TCGA-LIHC and IBD data sets. There is a performance gap between interpolation and GAN-based methods, and the SR method based on learning has a significant mapping advantage for complex gastrointestinal images. MoCoSR achieves the best performance among all evaluation metrics. CMRSR and MRESR cannot guarantee the output quality of mapping from HR back to LR, resulting in poor performance on complex 3D bowel data. Representatives for the qualitative evaluation are shown in Fig. 4.

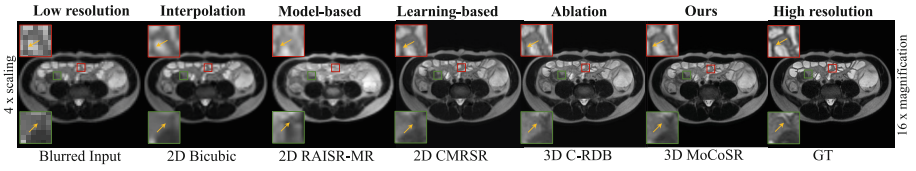

Fig. 4. Qualitative evaluation for SR on IBD dataset using representative methods of interpolation, model-based, learning-based, ablation, and MoCoSR.

Sensitivity Analysis: We evaluate if our method influences downstream analysis using the example of automatic scoring of Crohn's disease with existing deep networks. If features defining Crohn's disease are hidden by the method, this would affect disease scoring. We use a classifier with an attention mechanism similar to [22], trained on HR raw data. Our evaluation is based on the average possibility of normal and abnormal small bowel inflammation on MRI. The degree of small bowel inflammation on abnormal MRIs was classified by Radiologists as mild, moderate or severe. This outcome was compared against the results of the data constructed from different SR methods.

Complete results including LR degraded image, SR image reconstructed by MRESR, CMRSR, and MoCoSR, are shown in Table 3. We tracked and quantified the changes by performing a significance evaluation (t-test) based on p-values < 0.05. The ideal SR data can achieve classification results as close as possible to HR data with lower requirements. Our method obtains similar small-scale attenuation results on both healthy and abnormal samples. The p-value is larger than 0.05 for MoCoSR, *i.e.*, there is no statistically significant difference between the original and reconstructed data for the prediction results. The results of MRESR are volatile but present an unexpected improvement on healthy samples. CMRSR makes the predicted probability much lower than that of HR.

Discussion: According to the sensitivity analysis and comparison results, our MoCoSR method shows superior results compared to the forward adversarial reconstruction algorithms and encoder-decoder structures. Combining multi-scale image information in the feature space of different resolution image domains yields better results than inter-domain integration. The cycle consistency network splits the different resolution spaces and latent space, which facilitates the flexibility of the neural network to customize the MC according to the specific purpose and ensures consistency of the corrected data with the unpaired data. Furthermore, although these methods can obtain acceptable SSIM and PSNR, the key features used by the classifier for downstream tasks are potentially lost during the reconstructions. Conversely, the reconstruction result will implicitly cause domain shift. This leads to a distribution shift in the samples, which makes the disease prediction biased as shown in Fig. 5. The data generated by ours can

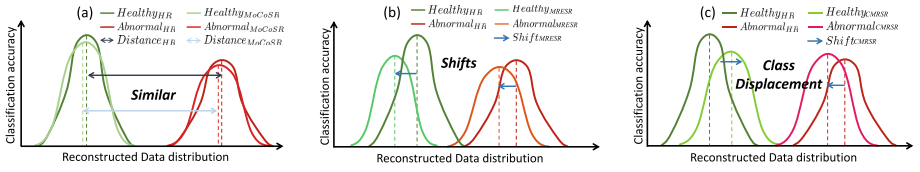

Fig. 5. Distribution relationships between reconstructed 3D bowel data and original HR data in a downstream Crohn's disease diagnosis task. (a) MoCoSR preserves diagnostic features and reconstructs a close representation of original data distribution. (b) The comparison method results in the loss and concealment of discriminative features. (c) Incorrectly reconstructed data misleads shifts in the distribution of SR data, which affects downstream task results.

Table 3. Crohn's disease classification performance on different 3D data. MoCoSR has a negligible effect on the downstream classification task as shown by high p-values in contrast to LR, MRESR, and CMRSR which produce significantly lower performance.

Data	Classification	Changes in/ Prediction	Significance p-value	CI 95% (Lower, Upper)
HR	Healthy	0.784	N/A	N/A
	Abnormal	0.730		
LR	Healthy	$-0.19^{*}\downarrow\downarrow$	<0.001	(0.13, 0.24)
	Abnormal	$-0.21^{*}\downarrow\downarrow$	<0.001	(0.14, 0.25)
MRESR [17]	Healthy	$-0.11^{*}\downarrow\downarrow$	<0.001	(0.05, 0.16)
	Abnormal	$-0.10^{*}\downarrow\downarrow$	0.002	(0.04, 0.15)
CMRSR [16]	Healthy	$+0.03\uparrow$	0.370	$(-0.08, 0.03)$
	Abnormal	$-0.08^{*}\downarrow$	0.012	(0.02, 0.13)
MoCoSR (ours)	Healthy	$-0.01\downarrow$	0.630	$(-0.04, 0.06)$
	Abnormal	$-0.02\downarrow$	0.561	$(-0.04, 0.07)$

reconstruct the results, retain likely all of the diagnostically valuable features, and maintain the original data distribution. The present sensitivity study is limited to the automatic classification from single domain and down-stream task framework, and future extensions will explore model-based and learning segmentation tasks across data domains and acquisitions.

4 Conclusion

MoCoSR is a DL-based approach to reconstruct high-quality SR MRI. MoCoSR is evaluated extensively and compared to the various image SR reconstruction algorithms on a public abdominal dataset, simulating different degrees of respiratory motion, and an IBD dataset with inherent motion. MoCoSR demonstrated superior performance. To test if our learned reconstruction preserves clinically relevant features, we tested on a downstream disease scoring method and found no decrease in disease prediction performance with MoCoSR.

Acknowledgements. This work was supported by the JADS programme at the UKRI Centre for Doctoral Training in Artificial Intelligence for Healthcare (EP/S023283/1) and HPC resources provided by the Erlangen National High Performance Computing Center (NHR@FAU) of the Friedrich-Alexander-Universität Erlangen-Nürnberg (FAU) under the NHR project b143dc. NHR funding is provided by federal and Bavarian state authorities. NHR@FAU hardware is partially funded by the German Research Foundation (DFG) - 440719683. Support was also received by the ERC - project MIA-NORMAL 101083647 and DFG KA 5801/2-1, INST 90/1351-1.

References

1. Gastrointestinal Unit Medical Services MGH, Andres, P.G., Friedman, L.S., et al.: Epidemiology and the natural course of inflammatory bowel disease. Gastroenterol. Clin. North Am. **28**(2), 255–281 (1999)
2. Sandler, R., Eisen, G.: Epidemiology of inflammatory bowel disease. In: Kirsner (ed.) Inflammatory Bowel Disease, p. 96 5th ed. WB Saunders, Philadelphia (2000)
3. Rosen, M.J., Dhawan, A., Saeed, S.A.: Inflammatory bowel disease in children and adolescents. JAMA Pediatrics. **169**(11), 1053–60 (2015)
4. Tielbeek, J.A., et al.: Grading Crohn disease activity with MRI: interobserver variability of MRI features, MRI scoring of severity, and correlation with Crohn disease endoscopic index of severity. AJR **201**(6), 1220–8 (2013)
5. Ebner, M., et al.: Point-spread-function-aware slice-to-volume registration: application to upper abdominal MRI super-resolution. In: Zuluaga, M.A., Bhatia, K., Kainz, B., Moghari, M.H., Pace, D.F. (eds.) RAMBO/HVSMR -2016. LNCS, vol. 10129, pp. 3–13. Springer, Cham (2017). https://doi.org/10.1007/978-3-319-52280-7_1
6. Zaitsev, M., Maclaren, J., Herbst, M.: Motion artifacts in MRI: a complex problem with many partial solutions. Magn. Reson. Imaging. **42**(4), 887–901 (2015)
7. Afaq, A., et al.: Pitfalls on PET/MRI. In: Seminars in Nuclear Medicine, vol. 51, pp. 529–39. Elsevier (2021)
8. Alansary, A., et al.: PVR: patch-to-volume reconstruction for large area motion correction of fetal MRI. IEEE Trans. Med. Imaging. **36**(10), 2031–44 (2017)
9. Wang, Z., Chen, J., Hoi, S.C.H.: Deep learning for image super-resolution: a survey. IEEE Trans. Pattern Anal. Mach. Intell. **43**(10), 3365–87 (2021)
10. Lim, B., Son, S., Kim, H., Nah, S., Mu Lee K.: Enhanced deep residual networks for single image super-resolution. In: CVPR, pp. 136–44 (2017)
11. Feng, C.-M., Yan, Y., Fu, H., Chen, L., Xu, Y.: Task transformer network for joint MRI reconstruction and super-resolution. In: de Bruijne, M., et al. (eds.) MICCAI 2021, Part VI. LNCS, vol. 12906, pp. 307–317. Springer, Cham (2021). https://doi.org/10.1007/978-3-030-87231-1_30
12. Feng, C.-M., Fu, H., Yuan, S., Xu, Y.: Multi-contrast MRI super-resolution via a multi-stage integration network. In: de Bruijne, M., et al. (eds.) MICCAI 2021, Part VI. LNCS, vol. 12906, pp. 140–149. Springer, Cham (2021). https://doi.org/10.1007/978-3-030-87231-1_14
13. Chen, Y., Shi, F., Christodoulou, A.G., Xie, Y., Zhou, Z., Li, D.: Efficient and accurate MRI super-resolution using a generative adversarial network and 3D multi-level densely connected network. In: Frangi, A.F., Schnabel, J.A., Davatzikos, C., Alberola-López, C., Fichtinger, G. (eds.) MICCAI 2018, Part I. LNCS, vol. 11070, pp. 91–99. Springer, Cham (2018). https://doi.org/10.1007/978-3-030-00928-1_11
14. Sánchez, I., Vilaplana, V.: Brain MRI super-resolution using 3D generative adversarial networks. arXiv preprint arXiv:1812.11440 (2018)
15. Georgescu, M.I., et al.: Multimodal multi-head convolutional attention with various kernel sizes for medical image super-resolution. In: Proceedings of the IEEE/CVF Winter Conference on Applications of Computer Vision, pp. 2195–205 (2023)
16. Zhao, M., Wei, Y., Wong, K.K.: A Generative Adversarial Network technique for high-quality super-resolution reconstruction of cardiac magnetic resonance images. Magn. Reson. Imaging. **85**, 153–60 (2022)
17. Do, H., Bourdon, P., Helbert, D., Naudin, M., Guillevin, R.: 7T MRI super-resolution with Generative Adversarial Network. Electronic Imaging. **2021**(18), 106–1 (2021)

18. Liu, J., Li, H., Huang, T., Ahn, E., Razi, A., Xiang, W.: Unsupervised representation learning for 3D MRI super resolution with degradation adaptation. arXiv preprint arXiv:2205.06891 (2022)
19. Wang, S., et al.: Joint motion correction and super resolution for cardiac segmentation via latent optimisation. In: de Bruijne, M., et al. (eds.) MICCAI 2021. LNCS, vol. 12903, pp. 14–24. Springer, Cham (2021). https://doi.org/10.1007/978-3-030-87199-4_2
20. Luo, Z., Huang, H., Yu, L., Li, Y., Fan, H., Liu, S.: Deep constrained least squares for blind image super-resolution. In: Proceedings of the IEEE/CVF Conference on Computer Vision and Pattern Recognition, pp. 17642–17652 (2022)
21. Mahapatra, D., Schüffler, P.J., Tielbeek, J.A., Makanyanga, J.C., Stoker, J., Taylor, S.A., et al.: Automatic detection and segmentation of Crohn's disease tissues from abdominal MRI. IEEE Trans. Med. Imaging. **32**(12), 2332–47 (2013)
22. Holland, R., Patel, U., Lung, P., Chotzoglou, E., Kainz, B.: Automatic detection of bowel disease with residual networks. In: Rekik, I., Adeli, E., Park, S.H. (eds.) PRIME 2019. LNCS, vol. 11843, pp. 151–159. Springer, Cham (2019). https://doi.org/10.1007/978-3-030-32281-6_16
23. He, K., Zhang, X., Ren, S., Sun, J.: Deep residual learning for image recognition. In: CVPR, pp. 770–778 (2016)
24. Taylor, S.A., et al.: Diagnostic accuracy of magnetic resonance enterography and small bowel ultrasound for the extent and activity of newly diagnosed and relapsed Crohn's disease (METRIC): a multicentre trial. Lancet Gastroenterol Hepatol. **3**(8), 548–58 (2018)
25. Romano, Y., Isidoro, J., Milanfar, P.: RAISR: rapid and accurate image super resolution. IEEE Trans. Comput. Imaging. **3**(1), 110–25 (2016)